PERGAMON

International Journal of Solids and Structures 40 (2003) 2343–2354

INTERNATIONAL JOURNAL OF SOLIDS and STRUCTURES

www.elsevier.com/locate/ijsolstr

Evolving crack patterns in thin films with the extended finite element method

J. Liang [a], R. Huang [b,1], J.H. Prévost [b,*], Z. Suo [a]

[a] *Department of Mechanical and Aerospace Engineering, Princeton Materials Institute, Princeton University, Princeton, NJ 08544, USA*

[b] *Department of Civil and Environmental Engineering, Princeton Materials Institute, Princeton University, Princeton, NJ 08544, USA*

Received 30 August 2002; received in revised form 14 January 2003

Abstract

This paper develops the extended finite element method (XFEM) to evolve patterns of multiple cracks, in a brittle thin film bonded to an elastic substrate, with a relatively coarse mesh, and without remeshing during evolution. A shear lag model describes the deformation in three dimensions with approximate field equations in two-dimensions. The film is susceptible to subcritical cracking, obeying a kinetic law that relates the velocity of each crack to its energy release rate. At a given time, the XFEM solves the field equations and calculates the energy release rate of every crack. For a small time step, each crack is extended in the direction of maximal hoop stress, and by a length set by the kinetic law. To confirm the accuracy of the XFEM, we compare our simulation to the exiting solutions for several simple crack patterns, such as a single crack and a set of parallel cracks. We then simulate the evolution of multiple cracks, initially in a small region of the film but of different lengths, showing curved crack propagation and crack tip shielding. Starting with multiple small cracks throughout the film, the XFEM can generate the well-known mud crack pattern.

Keywords: Crack patterns; Subcritical cracking; Thin films; Extended finite element method

1. Introduction

Many brittle solids are susceptible to subcritical cracking (Lawn, 1993). As shown in Fig. 1, a crack propagates at a value of energy release rate, G, smaller than the critical mechanical energy release rate, G_c, but remains stationary if G is smaller than the threshold value, G_{th}. Subcritical cracking manifests itself as environmental molecules assist in breaking the atomic bonds at the crack tip. The corrosive molecules correspond to those that will lower the surface tension and promote crack growth. This mechanism is widely observed in the failure of optical fibers and in microelectronic devices (He et al., 1998; Ma et al.,

* Corresponding author. Tel.: +1-609-258-5424; fax: +1-609-258-2760.
E-mail address: prevost@princeton.edu (J.H. Prévost).
[1] Present address: Aerospace Engineering and Engineering Mechanics Department, University of Texas at Austin, Austin, TX 78712-1085, USA.

0020-7683/03/$ - see front matter © 2003 Elsevier Science Ltd. All rights reserved.
doi:10.1016/S0020-7683(03)00095-7

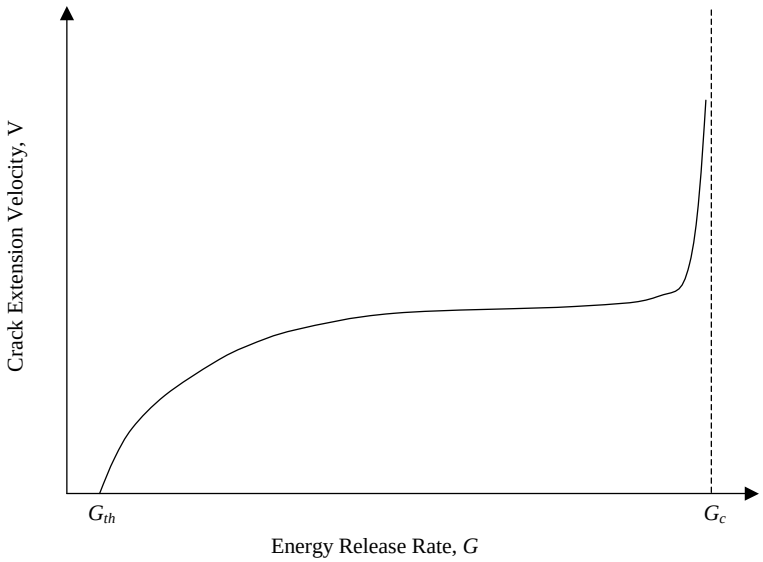

Fig. 1. A schematic diagram of the crack extension velocity versus the mechanical energy release rate for subcritical decohesion.

1998; Cook and Liniger, 1999). Under auspicious conditions, though not limited to subcritical decohesion, the cracking will develop very interesting and aesthetic patterns (Xia and Hutchinson, 2000; Argon, 1959; Néda et al., 2002; Dillard et al., 1994).

This paper studies crack pattern evolution in a brittle film susceptible to subcritical cracking. Fig. 2 illustrates the configuration. An elastic blanket film of thickness h is bonded to an elastic layer of thickness H. This structure sits above a rigid substrate. The elastic film is initially under uniform biaxial stress σ_0. Cracks pre-exist in the film. To describe subcritical crack growth, we prescribe a kinetic law that relates the crack velocity to the energy release rate.

We adopt a shear lag model to describe the deformation in three dimensions with approximate field equations in two-dimensions. The regular finite element method meshes the geometry of the crack and uses

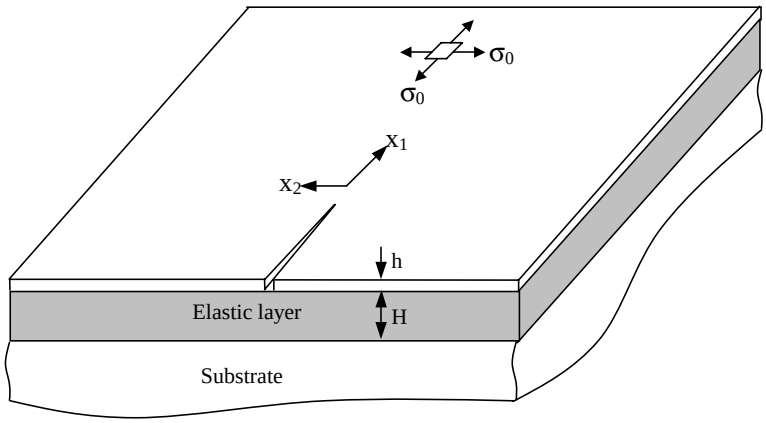

Fig. 2. An elastic thin film subjected to uniform strain on an elastic layer which in turn sits on top of a thick substrate. The film contains pre-existing crack.

a fine mesh near the crack tip. When the crack grows, remeshing is required. To circumvent these difficulties, we use the extended finite element method (XFEM), where discontinuous enrichment functions are added to the conventional finite element method to account for the presence of cracks, and singular enrichment functions are added to account for the crack tips (Belytschko and Black, 1999; Moës et al., 1999; Daux et al., 2000; Sukumar et al., 2003). The finite element software DYNAFLOW is used (Prévost, 2002). The advantages of the XFEM are that uniform and relatively coarse mesh can be employed while achieving excellent accuracy, and that no remeshing is required as cracks propagate. We present calculation results for several examples, illustrating patterns of various degree of complexity, from a single straight crack to the mud crack pattern.

2. Model

A two-dimensional shear lag model is adopted to study cracks in a thin film bonded to an elastic layer (Xia and Hutchinson, 2000). Similar models have been used to study cracking in a brittle film on a viscous underlayer (Huang et al., 2002; Liang et al., 2003; Lehner et al., 1981). The film surface coincides with the coordinate plane (x_1, x_2). The reference state is the film subjected to a uniform equal biaxial stress σ_0 in which the displacement field vanishes. At time t, the inplane displacement field measured relative to the reference state is $u_\alpha(x_1, x_2, t)$, where the Greek subscripts take on values of 1 and 2.

The film feels a shearing stress τ_α on the bottom face from the deformation of the elastic substrate. Force balance on a differential element of the film requires that the membrane stresses $\sigma_{\alpha\beta}$ satisfy

$$\sigma_{\alpha\beta,\beta} = \tau_\alpha / h, \tag{2.1}$$

where the comma signifies differentiation. We adopt the convention that repeated Greek subscript implies summation over 1 and 2. We model the film as an elastic, isotropic solid under the plane stress conditions:

$$\sigma_{\alpha\beta} = \frac{E}{1-v^2}[(1-v)\varepsilon_{\alpha\beta} + v\varepsilon_{\gamma\gamma}\delta_{\alpha\beta}] + \sigma_0\delta_{\alpha\beta}, \tag{2.2}$$

where E is Young's Modulus, v is Poisson's ratio, and $\delta_{\alpha\beta} = 1$ when $\alpha = \beta$ and $\delta_{\alpha\beta} = 0$ otherwise. The strains relate to the displacements as:

$$\varepsilon_{\alpha\beta}(u) = \frac{1}{2}(u_{\alpha,\beta} + u_{\beta,\alpha}). \tag{2.3}$$

We assume that the shear stresses τ_α are uniform across the thickness of the underlayer, and write

$$\tau_\alpha = \mu\frac{u_\alpha}{H}, \tag{2.4}$$

where μ is the shear modulus of the underlayer. Combining Eqs. (2.1)–(2.4), we obtain that

$$l^2\left[\frac{1}{2(1+v)}u_{\alpha,\beta\beta} + \frac{1}{2(1-v)}u_{\beta,\beta\alpha}\right] = u_\alpha, \tag{2.5}$$

where the length scale

$$l = \sqrt{\frac{hHE}{\mu}} \tag{2.6}$$

measures the decay distance of stress as a result of elastic relaxation. Using representative values, $h = 1.0$ μm, $H = 1$ μm, $E = 10^{11}$ N/m^2, and $\mu = 10^9$ N/m^2, $l = 10$ μm. This length is used to normalize the coordinates x_1 and x_2 in the simulation.

Time is introduced into this problem by prescribing a crack growth law. A representative relation between the crack velocity V and the energy release rate G takes the form:

$$V = V_0 \sinh\left[\beta\left(\frac{G}{G_{\text{th}}} - 1\right)\right], \tag{2.7}$$

where V_0 and β are parameters to fit experimental data. When $G < G_{\text{th}}$, the crack is assumed to be stationary; when $G > G_{\text{th}}$, the crack moves with a velocity according to Eq. (2.7). The parameters l and V_0 define a time scale

$$t_0 = \frac{l}{V_0}. \tag{2.8}$$

This time scale is used to normalize the time of evolution.

Once Eq. (2.5) is solved, the energy release rate is known, and Eq. (2.7) is used to update the crack tip position. Next, Eq. (2.5) is employed again to solve for the displacement field for the next time step, and the procedure repeats itself. The crack propagates in the direction of maximal hoop stress at the crack tip. See Appendix A for the procedures to compute the energy release rate and the direction of crack growth.

The problem has several dimensionless parameters:

$$\frac{EG_{\text{th}}}{\sigma_0^2 l}, \beta, \nu.$$

The first number is the threshold energy release rate relative to the elastic energy stored in the film, the second number is a material property characterizing the crack propagation velocity, and the third number is the Poisson's ratio.

3. Numerical approximation

3.1. Governing equations

The stress equilibrium equation in the film is coupled to the elastic relaxation in the underlayer as (from Eqs. (2.1) and (2.4)):

$$\sigma_{\alpha\beta,\beta} = \frac{\mu}{h}\frac{u_\alpha}{H} \quad \text{on } \Omega \tag{3.1}$$

and the constitutive relation in the film is given by Hooke's law:

$$\sigma_{\alpha\beta} = \sigma^{\text{i}}_{\alpha\beta} + \mathbf{E}_{\alpha\beta\gamma\delta}\varepsilon_{\gamma\delta}, \tag{3.2}$$

where $\mathbf{E}$ is the isotropic elasticity tensor (Eq. (2.2)), and $\sigma^{\text{i}}_{\alpha\beta}$ is the initial stress viz, $\sigma^{\text{i}}_{\alpha\beta} = \sigma_0\delta_{\alpha\beta}$. Usual traction and displacement boundary conditions prevail on the boundary of the film, viz,

$$\sigma_{\alpha\beta}n_\beta = \bar{t}_\alpha \quad \text{on } \Gamma_t, \tag{3.3}$$

$$u_\alpha = \bar{u}_\alpha \quad \text{on } \Gamma_u, \tag{3.4}$$

where $\mathbf{n}$ is the unit outward normal to the boundary $\Gamma = \partial\Omega$ of the film domain Ω, and Γ_t and Γ_u are the part of the boundary Γ on which traction and displacement are prescribed, respectively, ($\Gamma = \overline{\Gamma_t \cup \Gamma_u}; \Gamma_t \cap \Gamma_u = \phi$). The crack surface Γ_{c} is assumed to be traction-free, viz,

$$\sigma_{\alpha\beta}n_\beta = 0 \quad \text{on } \Gamma_{\text{c}+} \quad \text{and} \quad \Gamma_{\text{c}-}, \tag{3.5}$$

where $\Gamma_{\text{c}+}$ and $\Gamma_{\text{c}-}$ denote the two surfaces of the crack.

3.2. Weak form

The space of admissible displacement fields is defined by

$$U_u = \{\mathbf{u} \in V_u : \mathbf{u} = \bar{\mathbf{u}} \text{ on } \Gamma_u; \mathbf{u} \text{ discontinuous on } \Gamma_c\}, \tag{3.6}$$

where the space V_u is related to the regularity of the solution. Details on the matter may be found in Babuska and Rosenzweig (1972) and Grisvard (1985). Note that V_u allows for discontinuous functions across the crack line. The test functions space is defined similarly as

$$W_u = \{\mathbf{v} \in V_u : \mathbf{v} = 0 \text{ on } \Gamma_u; \mathbf{v} \text{ discontinuous on } \Gamma_c\}. \tag{3.7}$$

The weak form of the initial boundary value problem (Eqs. (3.1)–(3.5)) is given by

$$\int_\Omega \varepsilon(\mathbf{u}) : \mathbf{E} : \varepsilon(\mathbf{v})\,\mathrm{d}\Omega + \int_\Omega \frac{\mu}{hH}\mathbf{u}\cdot\mathbf{v}\,\mathrm{d}\Omega = \int_{\Gamma_t} \bar{\mathbf{t}}\cdot\mathbf{v}\,\mathrm{d}\Gamma - \int_\Omega \boldsymbol{\sigma}^{\mathrm{i}} : \varepsilon(\mathbf{v})\,\mathrm{d}\Omega \quad \forall \mathbf{v} \in W_u. \tag{3.8}$$

It is easily shown that the above are equivalent to the strong form, including the traction-free conditions on the crack faces (see e.g., Belytschko and Black (1999) for the special case of the stress equilibrium equation).

3.3. Finite element discretization

The model consists of a standard finite element discretization of standard basis functions which represent the smooth part of the solution, and of special basis functions which represent the discontinuity of **u** across the crack line and the stress concentration at the crack tip, as first suggested in Belytschko and Black (1999). Specifically, the approximation for **u** is assumed of the following form:

$$\mathbf{u}^h = \sum_A N^A(\mathbf{x})\left[\mathbf{u}^A + \sum_J \varphi_J(\mathbf{x})\mathbf{u}_J^A\right], \tag{3.9}$$

where $A =$ node number, $N^A(\mathbf{x})$ are the usual finite element basis functions (viz, $N^A(\mathbf{x}^B) = \delta^{AB}$), and $\varphi_J(\mathbf{x})$ are special enrichment functions used to model the discontinuity across the crack line and the crack tip. Specifically, XFEM models the crack by enriching the nodes whose basis function support intersects the crack line by using a discontinuous function which is referred to as a generalized Heaviside function $H(\mathbf{x})$, viz,

$$J = 1 \quad \varphi_1(\mathbf{x}) = H(x) = \begin{cases} +1 & \text{if } (\mathbf{x} - \mathbf{x}^*)\mathbf{e}_n \geqslant 0, \\ -1 & \text{otherwise,} \end{cases} \tag{3.10}$$

where $\mathbf{x}^*$ is the closest point to $\mathbf{x}$ on the crack Γ_c, and $\mathbf{e}_t$ and $\mathbf{e}_n$ are the unit tangent and normal vectors in the plane $\mathbf{e}_t \times \mathbf{e}_n = \mathbf{e}_3$ (see Moës et al. (1999)). To model the crack tip and also to improve the representation of the near field crack tip, XFEM models the crack tip by enriching the nodes whose basis function support intersects the crack tip by using the following functions:

$$\varphi_J(x) = \{\varphi_1, \varphi_2, \varphi_3, \varphi_4\} = \left[\sqrt{r}\cos\frac{\theta}{2}, \sqrt{r}\sin\frac{\theta}{2}, \sqrt{r}\sin\theta\sin\frac{\theta}{2}, \sqrt{r}\sin\theta\cos\frac{\theta}{2},\right], \tag{3.11}$$

(see Belytschko and Black (1999)) where (r, θ) are the local polar coordinates at the crack tip.

3.4. Semi-discrete finite element equations

Substitution of Eq. (3.9) into the weak form, results in the following system of semi-discrete equations:

$$\mathbf{K}\mathbf{u} = \mathbf{f}, \tag{3.12}$$

where $\mathbf{u} = \{\mathbf{u}^A, \mathbf{u}^A_J\}$ is the vector of nodal displacement unknowns. The matrix appearing in Eq. (3.12) is computed in the usual element-by-element fashion and assembled into the global matrix by using an expanded equation array which identifies nodes at which the special enrichment functions are used, viz, for a typical finite element, the contribution to $\mathbf{K}$ is computed as

$$\mathbf{k}^{ab} = \int_{\Omega^e} \mathbf{B}^{a^T} \mathbf{E} \mathbf{B}^b \, \mathrm{d}\Omega + \int_{\Omega^e} \frac{\mu}{Hh} \overline{B}^{a^T} \overline{B}^b \, \mathrm{d}\Omega, \tag{3.13}$$

where $a, b =$ local node numbers, Ω^e domain of element e, $\mathbf{B}^a =$ strain displacement matrix, viz,

$$\mathbf{B}^a = \begin{bmatrix} N^a_{,x} & 0 \\ 0 & N^a_{,y} \\ N^a_{,y} & N^a_{,x} \end{bmatrix} + \sum_J \begin{bmatrix} (N^a \varphi_J)_{,x} & 0 \\ 0 & (N^a \varphi_J)_{,y} \\ (N^a \varphi_J)_{,y} & (N^a \varphi_J)_{,x} \end{bmatrix} \tag{3.14}$$

and

$$\overline{\mathbf{B}}^a = \begin{bmatrix} N^a & 0 \\ 0 & N^a \end{bmatrix} + \sum_J \begin{bmatrix} N^a \varphi_J & 0 \\ 0 & N^a \varphi_J \end{bmatrix}, \tag{3.15}$$

where $J = 1$ if the element intersects the crack line, $J = 4$ if the crack tip is within the element, and $J = 0$ otherwise. Special quadratures are used to integrate Eq. (3.13) when $J \neq 0$ (see e.g., Moës et al. (1999)). The element contribution to the force vector is computed as

$$\mathbf{f}^a = -\int_{\Omega^e} \mathbf{B}^{a^T} \sigma^{\mathrm{i}} \, \mathrm{d}\Omega. \tag{3.16}$$

4. Results and discussion

4.1. A single straight crack moving in a blanket film

To confirm the accuracy of the XFEM, this and the next examples compare our simulation with the solution in Xia and Hutchinson (2000). We place a small crack of initial length $a_0 = 0.125l$ at the middle of the left boundary of our $12l$ by $12l$ computational cell. Zero normal displacement is prescribed at all four cell boundaries. The element size is $0.02l$. We use $\beta = 1.0$ and $G_{\mathrm{th}} = 0.35\sigma_0^2 l/E$.

Fig. 3 shows the results. In Fig. 3a, we compare the energy release rate, G, calculated using the XFEM to those obtained by Xia and Hutchinson (2000) using an integral equation approach. The trend in the results reflects the condition that when the ratio $a/l > 1.0$, the energy release rate is close to the asymptote value (Xia and Hutchinson, 2000)

$$G = \sqrt{1 - \nu^2} \frac{\sigma_0^2 l}{E}, \quad a/l \to \infty. \tag{4.1}$$

In Fig. 3b, we plot the crack propagation velocity, V, as a function of the crack length. The XFEM solution is in quite good agreement with those of Xia and Hutchinson (2000). However, because of the hyperbolic sine function in the velocity expression Eq. (2.7), small errors in G are magnified in V.

4.2. Parallel and sequential cracking of semi-infinite cracks in a blanket film

As another check of the XFEM code, we try to reproduce the results from Xia and Hutchinson (2000) for an infinite array of equally spaced semi-infinite cracks with tips aligned evenly and parallel to each other (parallel cracking), and of semi-infinite cracks advancing midway between previously formed infinite cracks

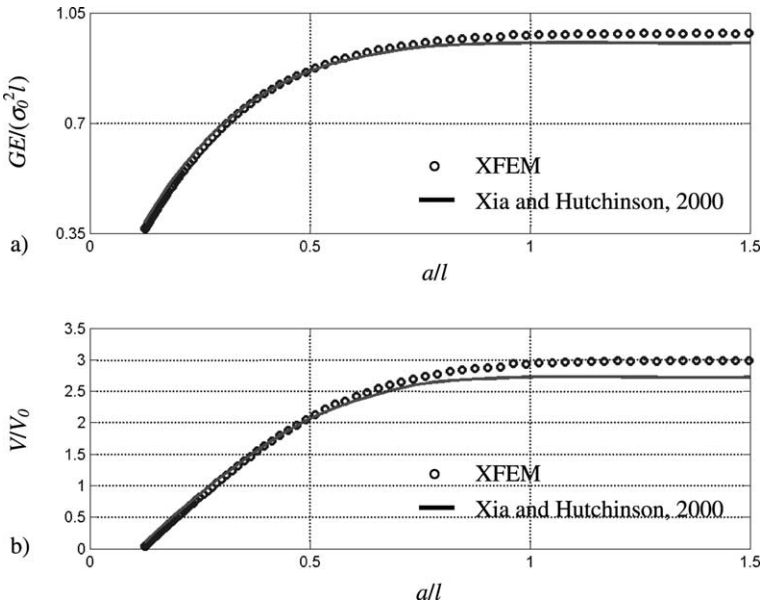

Fig. 3. Moving center crack in a blanket film. (a) Normalized energy release rate versus normalized crack length. (b) Normalized crack extension velocity versus normalized crack length.

(sequential cracking). We employed periodic conditions at the boundaries parallel to the cracks and zero normal displacement conditions at the boundaries perpendicular to the cracks. The crack length is taken to be half the length of the cell. The cell length is set to be $10l$ while the cell width is varied. The element size used is $0.02l$.

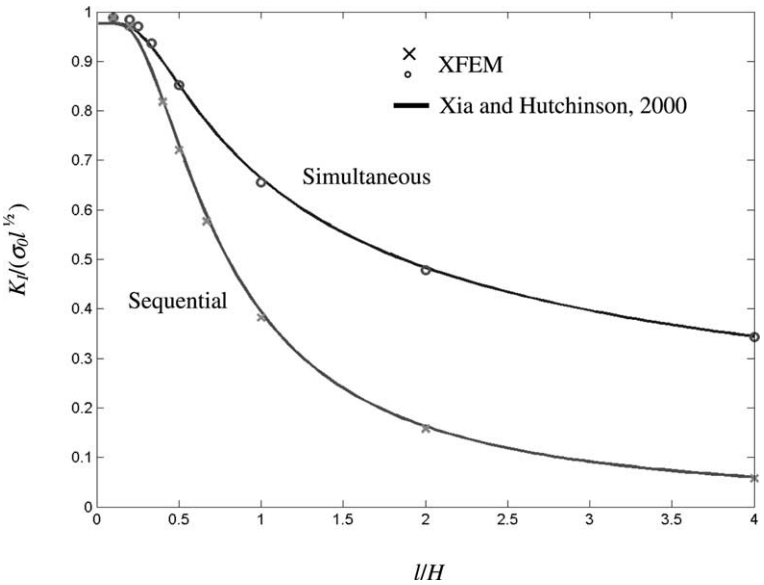

Fig. 4. Normalized stress intensity factor versus normalized inverse crack spacing for simultaneous and sequential cracking.

The plot in Fig. 4 demonstrates that the XFEM program produces results in good agreement with those given in Xia and Hutchinson (2000). This example concludes our testing of the XFEM code. The next two examples will discuss the different crack patterns that may emerge from thin film cracking.

4.3. Multiple cracks of different lengths moving in a blanket film

Fig. 5a shows the crack arrangement and the contour plot of the mean stress at $t/t_0 = 0$. Cracks a and e have initial length $0.5l$, b and d have $1.0l$, and c has $0.75l$. The spacing between cracks is $0.5l$. We employed a $15l$ by $15l$ cell with element size $0.0495l$. We set $\beta = 0.1$ and $G_{\text{th}} = 0.042\sigma_0^2 l/E$. There is a large region of relaxation in the wake of the cracks.

Fig. 5b shows the crack pattern at $t/t_0 = 1.0$. Cracks diverge from each other. Crack c, being the middle of the five cracks, should experience only mode I loading conditions and move straight. However, it is shorter than its two neighboring cracks. Consequently, it lies in the wake of cracks b and d. It moves a tiny amount initially but quickly gets trapped in the wake of its two much faster moving immediate neighbors. Therefore, it does not move after the first time step.

Cracks b and d repel each other and turn away from the center of the blanket film. The straight cracks would experience the mix-mode loading condition. The cracks propagate in a direction to make $K_{\text{II}} = 0$. Initially, K_{II} is positive for crack b and negative for crack d. This indicates that crack b should turn downwards while crack d should turn upwards as they do in Fig. 5b. But after four or five time steps, both cracks stop turning and start to propagate in a diagonal straight path. This is because the crack tips, having moved far enough apart from each other, do not feel each other's presence. The loading condition becomes pure Mode I again despite the fact that the crack is at an angle to the x_1 and x_2 coordinate axes. This is only true for equal biaxial loading conditions as is the case for this example.

Cracks a and e also move away from the center of the film. They are the shortest cracks, and their tips are partially shielded from the residual loading by the longer crack next to them. As a result, they have much slower velocity than cracks b and d and do not elongate very much. There is a clear asymmetry at the crack tip; thus, mix-mode loading applies. K_{II} for crack a is positive while K_{II} for crack e is negative. As a result, crack a turns downwards, and crack e turns upwards as shown in Fig. 5b.

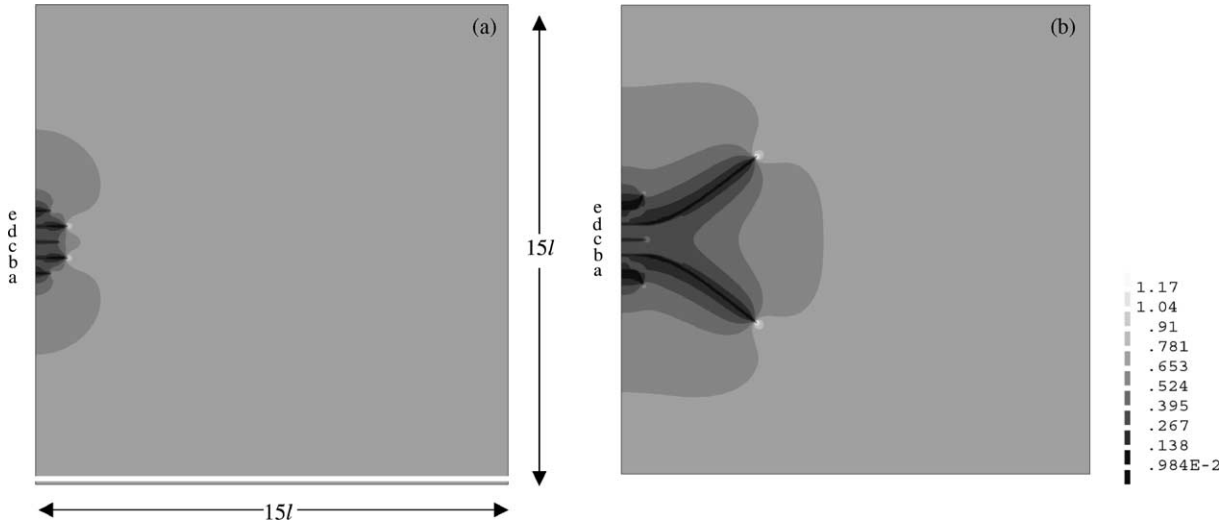

Fig. 5. Mean stress, normalized by the initial biaxial stress, contour plot of multiple moving center cracks of different initial lengths. The grayscale is linear from 0.0 to 1.3 and applies to both figures a and b. (a) At $t/t_0 = 0$, (b) at $t/t_0 = 1.0$.

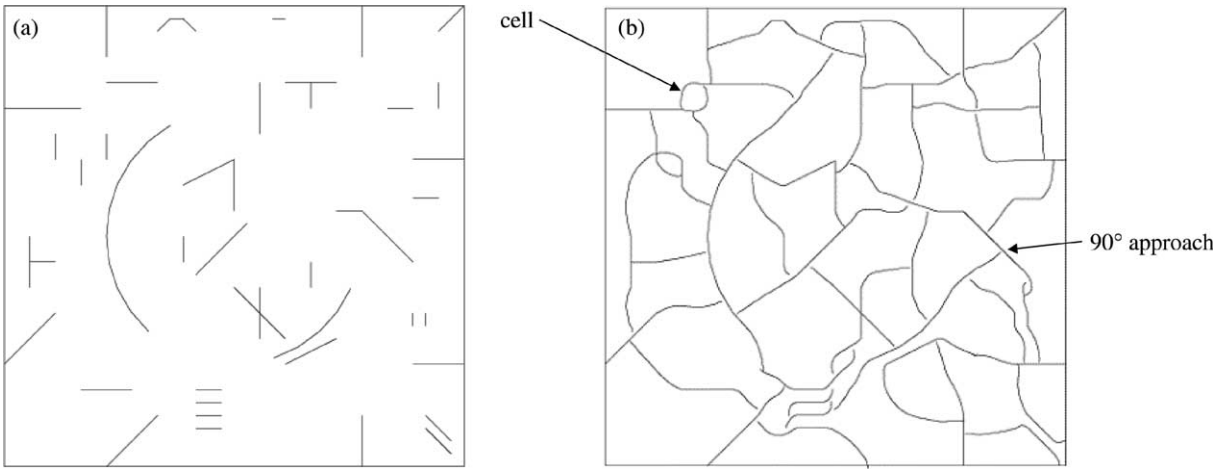

Fig. 6. Mud crack pattern: (a) $t/t_0 = 0$, (b) $t/t_0 = 1.0$.

4.4. Mud cracks in a blanket film

The mud crack pattern is shown in Fig. 6. The computational cell size is $9l$ by $9l$, and the element size is $0.05l$. Fig. 6a shows the initial distribution of cracks that we prescribe in the blanket film. Fig. 6b presents the final crack pattern. Crack tip motion is stopped if it is about to intersect any part of another crack. This criterion is based on the assumption that cracks are free surface defects such that parallel crack walls are discontinuities in the film. Thus, an approaching crack tip has no way to cross over the discontinuity. We could also have prescribed other criteria for the intersections, but choose not to at this point. Consequently, from Fig. 6b, we see many instances where the motion of a crack tip is terminated near a crack line that was initially there or created by other cracks. The approximate nature of this termination condition also leads to the small spacing between the crack tip and the nearest crack line. Another interesting point to make is that the cracks tips approach another crack at right angles. This is true for all but one of the cracks in Fig. 6b because pure Mode I condition is expected at this incident angle. In one case where this is not true in Fig. 6b, we believe that it is due to numerical inaccuracies. If the crack growth increment had been smaller, the angle would be 90° at the junction.

As the crack tips approach each other, the cracks must begin to deviate from their former course due to mode mixity. Every time two tips close enough to each other move together, they are expected to turn towards each other. The tip motion would then cease when the tip meets the other crack. This sequence of events leads to the many small cells that are seen in Fig. 6b. Finally, we observe that when two cracks are parallel to each other, then their tips will diverge from each other if the tips are close enough to the other crack. This is similar to the observation in Section 4.3.

5. Conclusion

We have demonstrated a numerical method to evolve complex crack patterns in a brittle thin film susceptible to subcritical cracking. The XFEM obtains accurate solutions of the stress intensity factors. Our results compare well with those published by Xia and Hutchinson (2000). This demonstrates the reliability of the procedure. Furthermore, we use the crack pattern from multiple cracks of different lengths moving in a blanket film to explain how crack propagation direction may be predicted based on the stress intensity

factors. Finally, the mud crack pattern shows that the crack tips intersect crack lines at right angles, and that two crack tips approaching each other will bypass each other and then be attracted to each other to form a small cell. However, two crack tips traveling parallel to each other tend to repel.

Acknowledgements

This work is supported by the National Science Foundation through grants CMS-9820713 and CMS-9988788 with Drs. Ken Chong and Jorn Larsen-Basse as the program directors.

Appendix A

This appendix describes how we compute the energy release rate at the crack tip and how we determine the direction of crack growth in the present study.

For an elastic body without any body force, there exists a path-independent integral (Rice, 1968)

$$J = \int_C \left(W\delta_{1\alpha} - \sigma_{\alpha\beta}\frac{\partial u_\beta}{\partial x_1} \right) n_\alpha \, \mathrm{d}s, \tag{A.1}$$

where C is a contour circling the crack tip in the counter-clockwise direction with n_j as its outward unit normal and $\mathrm{d}s$ as its arc length, and $W = (1/2)\sigma_{\alpha\beta}(\partial u_\alpha/\partial x_\beta)$ is the strain energy density. The J-integral coincides with the energy release rate at the crack tip, i.e., $G = J$. To compute the energy release rate numerically, however, it is more convenient to use the domain form of the J-integral (Li et al., 1985; Moran and Shih, 1987; Shih and Asaro, 1988)

$$J = \int_A \left(\sigma_{\alpha\beta}\frac{\partial u_\alpha}{\partial x_1} - W\delta_{1\beta} \right) \frac{\partial q}{\partial x_\beta} \, \mathrm{d}A, \tag{A.2}$$

where A is the area bounded by the contour C and the crack faces up to the crack tip, and q is an arbitrary smooth weighting function with the value of unity at the crack tip and the value of zero on the contour and values varying smoothly from zero to one inside the contour.

For an elastic body with a body force b_α (i.e., $\sigma_{\alpha\beta,\beta} + b_\alpha = 0$), however, the J-integral is not path-independent, and the energy release rate becomes

$$G = \lim_{C\to 0}\{J(C)\}, \tag{A.3}$$

where the limit implies that the contour C is shrunk onto the crack tip. In the present study, from Eqs. (2.1) and (2.4), the body force is

$$b_\alpha = -\frac{\mu}{hH}u_\alpha. \tag{A.4}$$

To compute the energy release rate for problems with body forces, we define a new integral (Huang et al., 2002)

$$J_B = \int_C \left(W\delta_{1\beta} - \sigma_{\alpha\beta}\frac{\partial u_\alpha}{\partial x_1} \right) n_\beta \, \mathrm{d}s - \int_A b_\alpha \frac{\partial u_\alpha}{\partial x_1} \, \mathrm{d}A. \tag{A.5}$$

It can be shown that the integral J_B is independent of the choice of the contour C and, indeed, it coincides with the energy release rate G. Integrals similar to (A.5) have been used to compute the dynamic energy release rate in dynamic fracture mechanics (Freund, 1990; Nakamura et al., 1985). Following Li et al. (1985), we obtain the domain form of J_B

$$J_B = \int_A \left[\left(\sigma_{\alpha\beta} \frac{\partial u_\alpha}{\partial x_1} - W\delta_{1\beta} \right) \frac{\partial q}{\partial x_\beta} - b_\alpha \frac{\partial u_\alpha}{\partial x_1} q \right] \mathrm{d}A. \tag{A.6}$$

For a general two-dimensional mixed mode problem, the relationship between the energy release rate and the stress intensity factors is

$$G = \frac{K_{\mathrm{I}}^2}{E^*} + \frac{K_{\mathrm{II}}^2}{E^*}, \tag{A.7}$$

where $E^* = E$ for plane stress problems and $E^* = E/(1-\nu^2)$ for plane strain problems. To extract the individual stress intensity factors, K_{I} and K_{II}, we use the domain form of the interaction integral (Shih and Asaro, 1988; Yau et al., 1980). Consider two states: state 1 $(\sigma_{ij}^{(1)}, u_i^{(1)})$ corresponds to the actual state of interest, and state 2 $(\sigma_{ij}^{(2)}, u_i^{(2)})$ is an auxiliary state which will be chosen as the asymptotic fields for mode I and mode II, respectively. State 1 has a body force, and state 2 has no body force. The J_B-integral for the sum of the two states is

$$J_B^{(1+2)} = J_B^{(1)} + J_B^{(2)} + M^{(1,2)}, \tag{A.8}$$

where $M^{(1,2)}$ is the interaction integral of the two states

$$M^{(1,2)} = \int_A \left[\left(\sigma_{\alpha\beta}^{(1)} \frac{\partial u_\alpha^{(2)}}{\partial x_1} + \sigma_{\alpha\beta}^{(2)} \frac{\partial u_\alpha^{(1)}}{\partial x_1} - W^{(1,2)}\delta_{1\beta} \right) \frac{\partial q}{\partial x_\beta} - b_\alpha^{(1)} \frac{\partial u_\alpha^{(2)}}{\partial x_1} q \right] \mathrm{d}A \tag{A.9}$$

and $W^{(1,2)}$ is the interaction strain energy

$$W^{(1,2)} = \sigma_{\alpha\beta}^{(1)} \frac{\partial u_\alpha^{(2)}}{\partial x_\beta} = \sigma_{\alpha\beta}^{(2)} \frac{\partial u_\alpha^{(1)}}{\partial x_\beta}. \tag{A.10}$$

Combining the relationships, $G = J_B$, $G^{(1+2)} = G^{(1)} + G^{(2)}$ (A.7) and (A.8), the interaction integral relates to the stress intensity factors as

$$M^{(1,2)} = \frac{2}{E^*} \left(K_{\mathrm{I}}^{(1)} K_{\mathrm{I}}^{(2)} + K_{\mathrm{II}}^{(1)} K_{\mathrm{II}}^{(2)} \right). \tag{A.11}$$

Choosing the auxiliary state as Mode I asymptotic field with $K_{\mathrm{I}}^{(2)} = 1$ and $K_{\mathrm{II}}^{(2)} = 0$ gives the mode I stress intensity factor of the actual state

$$K_{\mathrm{I}}^{(1)} = \frac{E^*}{2} M^{(1,\text{Mode I})}. \tag{A.12}$$

Similarly choosing the auxiliary state as Mode II asymptotic field with $K_{\mathrm{I}}^{(2)} = 0$ and $K_{\mathrm{II}}^{(2)} = 1$ gives the mode II stress intensity factor of the actual state

$$K_{\mathrm{II}}^{(1)} = \frac{E^*}{2} M^{(1,\text{Mode II})}. \tag{A.13}$$

In the present study, we compute the stress intensity factors using the interaction integral and then compute the energy release rate based on (A.7). With both the stress intensity factors known, the direction of the crack growth is determined by using the maximum circumferential stress criterion (Erdogan and Sih, 1963). The circumferential stress near the crack tip is

$$\sigma_{\theta\theta}(r,\theta) = \frac{1}{\sqrt{2\pi r}} \cos^2(\theta/2)[K_{\mathrm{I}} \cos(\theta/2) - 3K_{\mathrm{II}} \sin(\theta/2)], \tag{A.14}$$

where (r,θ) are the local polar coordinates at the crack tip. The maximum circumferential stress occurs at the angle θ_p, given by

$$\tan\left(\frac{\theta_p}{2}\right) = \frac{-2K_{II}/K_I}{1+\sqrt{1+8(K_{II}/K_I)^2}}. \tag{A.15}$$

This direction is taken to be the direction of crack growth.

References

Argon, A.S., 1959. Surface cracks on glass. Proceedings of the Royal Society of London 250, 472–481.

Babuska, I., Rosenzweig, M., 1972. A finite element scheme for domains with corners. Numerical Mathematics 20, 1–21.

Belytschko, T., Black, T., 1999. Elastic crack growth in finite elements with minimal remeshing. International Journal for Numerical Methods in Engineering 45, 601–620.

Cook, R.F., Liniger, E.C., 1999. Stress-corrosion cracking of low-dielectric-constant spin-on-glass thin films. Journal of the Electrochemical Society 146, 4439–4448.

Daux, C., Moës, N., Dolbow, J., Sukumar, N., Belytschko, T., 2000. Arbitrary branched and intersecting cracks with the extended finite element method. International Journal for Numerical Methods in Engineering 48, 1741–1760.

Dillard, D.A., Hinkley, J.A., Johnson, W.S., St. Clair, T.L., 1994. Spiral tunneling cracks induced by environmental stress cracking in LARC-TPI adhesives. Journal of Adhesion 44, 51–67.

Erdogan, F., Sih, G., 1963. On the crack extension in plates under plane loading and transverse shear. Journal of Basic Engineering 85, 519–527.

Freund, L.B., 1990. Dynamic Fracture Mechanics. Cambridge University Press.

Grisvard, P., 1985. Elliptic Problems in Nonsmooth Domains. Pitman Publishing, Inc., Boston.

He, J., Morris, W.L., Shaw, M.C., Mather, J.C., Sridhar, N., 1998. Reliability in large area solder joint assemblies and effects of thermal expansion mismatch and die size. International Microelectronics and Packaging Society 21, 297–305.

Huang, R., Prévost, J.H., Suo, Z., 2002. Loss of constraint on fracture in thin film structures due to creep. Acta Materialia 50, 4137–4148.

Lawn, B., 1993. Fracture of Brittle Solids. Cambridge University Press.

Lehner, F.K., Li, V.C., Rice, J.R., 1981. Stress diffusion along rupturing plate boundaries. Journal of Geophysical Research 86, 6155–6169.

Li, F.Z., Shih, C.F., Needleman, A., 1985. A comparison of methods for calculating energy release rates. Engineering Fracture Mechanics 21, 405–421.

Liang, J., Huang, R., Prévost, J.H., Suo, Z., 2003. Concomitant thin film cracking and underlayer creep. Experimental Mechanics, submitted for publication.

Ma, Q., Xie, J., Chao, S., El-Mansy, S., McFadden, R., Fujimoto, H., 1998. Channeling cracking technique for toughness measurement of brittle dielectric thin films on silicon substrate. Materials Research Society Symposium Proceedings 516, 331–336.

Moës, N., Dolbow, J., Belytschko, T., 1999. A finite element method for crack growth without remeshing. International Journal for Numerical Methods in Engineering 46, 131–150.

Moran, B., Shih, C.F., 1987. Crack tip and associated domain integrals from momentum and energy balance. Engineering Fracture Mechanics 27, 615–642.

Nakamura, T., Shih, C.F., Freund, L.B., 1985. Computational methods based on an energy integral in dynamic fracture. International Journal of Fracture 27, 229–243.

Néda, Z., Leung, K.-t., Józsa, L., Ravasz, M., 2002. Spiral cracks in drying precipitates. Physical Review Letters 88, 095502-1–095502-4.

Prévost, J.H., 2002. DYNAFLOW: A Nonlinear Transient Finite Element Analysis Program. Princeton University, 1981.

Rice, J.R., 1968. A path-independent integral and the approximate analysis of strain concentration by notches and cracks. ASME Journal of Applied Mechanics 35, 379–386.

Shih, C.F., Asaro, R.J., 1988. Elastic-plastic analysis of cracks on bimaterial interfaces: Part I. Small scale yielding. Journal of Applied Mechanics 55, 299–316.

Sukumar, N., Srolovitz, D.J., Baker, T.J., Prévost, J.H., 2003. Brittle fracture in polycrystalline microstructures with the extended finite element method. International Journal for Numerical Methods in Engineering 56, 2015–2037.

Xia, Z.C., Hutchinson, J.W., 2000. Crack patterns in thin films. Journal of the Mechanics and Physics of Solids 48, 1107–1131.

Yau, J., Wang, S., Corten, H, 1980. A mixed-mode crack analysis of isotropic solids using conservation laws of elasticity. Journal of Applied Mechanics 47, 335–341.